Asian Journal of Chemistry; Vol. 37, No. 7 (2025), 1601-1613

ASIAN JOURNAL OF CHEMISTRY

https://doi.org/10.14233/ajchem.2025.33712

A Remedy for Global Warming through the Effective Use of Waste Dye Effluents for the Synthesis of $AlSiO_4$ Solid Acid Catalysts with Carbon Dioxide Decomposition

S. Senthil Kumar[1], Arjun Sunil Rao[2,*], K. Lakshmikandhan[3], S. Boobalan[1] and Basavaraj S. Sannakashappanavar[4]

[1]Department of Physics, CMS College of Engineering and Technology, Coimbatore-641032, India
[2]Department of Electronics and Communication Engineering, Manipal Institute of Technology (MIT), Manipal Academy of Higher Education (MAHE) Manipal, Udupi-576104, India
[3]Department of Chemistry, CMS College of Engineering and Technology, Coimbatore-641032, India
[4]Department of Electronics and Communication Engineering, Dayananda Sagar College of Engineering, Bengaluru-560078, India

*Corresponding authors: E-mail: arjun.rao@manipal.edu

Received: 22 March 2025; *Accepted*: 27 May 2025; *Published online*: 30 June 2025; AJC-22034

Global concern about its rising levels in the atmosphere has led to the search for novel strategies to decrease CO_2 productions. In this regard, this article presents a new type of catalyst for spontaneous decomposition of CO_2. Novel $AlSiO_4$ mesoporous solid acid catalysts are synthesized by different type of dye molecules as templates like anionic dye (Congo red ($AlSiO_4$-15), brilliant yellow ($AlSiO_4$-22) and cationic dye (rhodamine-B ($AlSiO_4$-13R)), nitroso dye (naphthol green-B ($AlSiO_4$-13N)). Here, harmful templates were avoided by using waste dye effluents as an appropriate template for the solid acid catalyst manufacturing process rather than traditional templates. Waste dye effluents were converted into a useful product and applied for environmental remedy. The carbon dioxide breakdown reaction uses the produced solid acid catalysts and was carried out in a recently developed U-type catalytic reactor. The catalytic bed was filled with solid acid catalysts that breakdown CO_2 into O_2, CO and carbon. The catalysts significantly lower the activation energy of CO_2 gas at room pressure and low temperature.

Keywords: Aluminosilicates, Dye templates, Solid acid catalyst, CO_2 decomposition, Low temperature.

INTRODUCTION

A significant effort has been made to break down carbon dioxide because of climate change and global warming [1,2]. The primary technology in the energy sector is carbon capture and storage (CCS), while there are numerous more options. This process includes capturing, compressing, transporting and safely depositing CO_2. And the last stage comprises (i) post-combustion, (ii) pre-combustion and (iii) oxy-fuel combustion technologies. It mostly depends on the location and method of the CO_2 collecting process. Post-combustion is one of the finest solutions for retrofitting existing power facilities. Cryogenics, membrane based technologies, wet absorption and dry adsorption are a few possible post-combustion routes. While each of them has pros and cons, the primary problem of most of them is their high cost and energy consumption [3].

Although absorption is the most well-known and effective method of separating CO_2, there are still concerns about how this process may affect the environment that need to be addressed [4]. Direct breakdown of CO_2 into CO has an advantage over widely used chemical and physical processes in terms of CO development, which is a feedstock in the chemical sector [5,6]. This technique is very endothermic and requires a high operating temperature (eqns. 1 and 2), as demonstrated by the enthalpy change of CO_2 decomposition [7].

$$CO_2 \rightarrow CO + \frac{1}{2}O_2 \qquad (1)$$
$$\Delta H = 2.9 \text{ eV per molecule } (283.3 \text{ KJ mol}^{-1})$$

$$CO_2 \rightarrow CO + O \qquad (2)$$
$$\Delta H = 5.5 \text{ eV per molecule } (532.3 \text{ KJ mol}^{-1})$$

In thermal method, the CO_2 decomposition needs more temperature for the formation of CO and O_2 (2000 K) [8,9].

Since this technology has the potential to the lower related costs, there is now a growing awareness of adsorption methods employing solid sorbents that can reversibly capture CO_2. This justification states that the usage of solid adsorbents has more capacity and selectivity, takes less energy for the regeneration step and is simpler to handle when compared to alternative post-combustion CO_2 collection techniques [10]. For breakthrough innovations to be realized, novel materials with higher CO_2 decomposition ability, selectivity and robustness must be developed. Common sorbents include lithium zirconates, zeolites, hydrotalcites, activated carbons, molecular sieves and calcium oxides [11-13]. Materials rich in carbon content are seen to be among the most favourable adsorbents due to their low cost, vast surface area, high flexibility to surface functionalization and porous structure and comparative ease of regeneration. Since CO_2 adsorption on carbon materials is weak and physical, these adsorbents exhibit a poor degree of selectivity and are temperature sensitive [14].

With pore sizes ranging from 2 to 50 nm, mesoporous solid acid is a more important material than microporous and other materials [15,16]. The porous materials are further classified into amorphous and crystalline. Aluminosilicate is a crystalline solids, this crystalline solid acid catalyst has main role in adsorption, sensor, catalysis and particularly in hydrocarbon conversion [17]. Mesoporous materials has a variety of applications by the reason of their manageable thermal stability, well-ordered pores and pore volume, surface area, active acid sites and easiness for regeneration [18]. In mesoporous material the vacant sites are arranged in a comparatively regular three-dimensional hexagonal arrangement [19]. Several organic hydrocarbons and surfactants are used as a structure directing agent in the elegant preparation of molecular sieves [20-22]. In most of the cases, the resultant materials are in a disordered mesoporous matrix and it has been suggested that the disordered mesopores in such compounds are created by non-templating structure-directing mechanism [23]. Generally, the properties of the porous material is mainly depends on its templates.

In present work, dye molecules are utilized as a structure directing agent; it is a new kind of move towards the synthesizing of nonporous solid acid catalyst. Anionic (Congo red), cationic (rhodamine-B) and nitroso dyes are used as a template molecule. Using this dye template, meso-structured aluminosilicate materials can be developed. The impact of the template on the physical and chemical characteristics of the resulting catalysts is investigated using a range of analytical and spectroscopic methods. In future, the industrial waste dye solution can be used as an alternative in support of template for solid acid catalyst synthesize and remove the same. The waste dye effluent can be used as a positive creation. However, decomposition of CO_2 over solid acid catalyst at low temperature is not yet reported. This study's objective is to assess the impact of CO_2 breakdown utilizing four distinct kinds of mesoporous solid acid catalysts. In this light, the present study contributes to comprehend the effect of packed solid acid catalysts on gas phase processes involving CO_2 breakdown and to attain the maximum O_2 and CO selectivity. It has been built and proven to convert CO_2 into CO, oxygen and carbonaceous compounds using a packed catalytic bed reactor. The packed catalytic bed encourages the conversion of CO_2 into CO and oxygen, according to a typical outcome.

EXPERIMENTAL

Mesoporous solid acid catalyst was prepared using $AlCl_3$ (98% Merck), sodium metasilicate (Loba Chemie), Congo red (Loba Chemie), brilliant yellow (Loba Chemie), rhodamine-B (Loba Chemie), naphthol green-B (Loba Chemie) and distilled water. In this work, two anionic, one cationic and one nitroso dyes were used as a template molecule and its physical properties are listed in Table-1.

Preparation of mesoporous solid acid catalysts: In a standard method, 13.5 g of $AlCl_3$ was added to 17.4 g of an anionic dye (Congo red) solution had been rapidly shaken. The mixture was allowed to precipitate entirely for a day after 28.5 g of sodium silicate powder was added and the liquid was magnetically swirled for 30 min. The template had the effect of keeping the gel's pH at 8.0. To get rid of all the unreacted material from the combination, the finished product was repeatedly cleaned with distilled water. The sample was then baked in a hot air oven for 3 h at 120 ºC. After that, the mixture was calcined at 900 ºC in an open environment until the catalyst's surface was free of all organic and undesired templates. The preparation of the other dye templated components (brilliant yellow and naphthol green-B) follows a similar process as described above. The template's concentration was 0.25.

Characterization: XRD (model: D8 Advance, Bruker, Cu$K\alpha$ radiation) was utilized to evaluate the mesophase arrangement and crystallinity of the samples. A Jasco 410 FT-IR type spectrophotometer was utilized to obtain the Fourier transform infrared (FT-IR) spectrum using KBr pellet. TGA Q500 V20.10 Build 36 instrument was utilized to assess the sample's thermal stability at a rate of 20 ºC/min. In the temperature range of 25 to 800 ºC, the data was acquired using Chemisoft TPx V1.02 instrument and the TPD-NH_3 desorption curve was recorded at a rate of 20º/min. Temperature-programmed desorption (TPD) tests employed helium flow (30 mL/min) and the quantity of desorbed ammonia was recorded using a TCD detector. The nitrogen adsorption-desorption isotherm at 77 K was used to investigate the textural characteristics of catalyst.

TABLE-1
SUMMARY OF PHYSICAL PROPERTIES OF DYE TEMPLATES

Nature of dye	Dye	m.f.	Molar mass (g/mol)
Anionic dye	Congo red (CR)	$C_{32}H_{22}N_6O_6S_2Na_2$	696.665
Anionic dye	Brilliant yellow (BY)	$C_{26}H_{18}N_4O_8S_2Na_2$	624.560
Cationic dye	Rhodamine-B (Rh-B)	$C_{28}H_{31}N_2O_3Cl$	479.020
Nitroso dye	Napthol green-B (NG-B)	$C_{30}H_{15}N_3O_{15}S_3FeNa_3$	878.450

New catalytic reactor set up: For this, a novel U-shaped catalytic reactor was developed (Fig. 1). A U-shaped parallel continuous flow reactor was used to assess the catalytic activity. After the samples have been compressed, crushed and ground into a fine powder, solid acid catalyst was added to the reactor. To monitor the temperature of the heated plate, a thermometer was utilized and the reactor was immersed in motor oil. The reactor's inlet was connected to a 99.6% pure CO_2 cylinder and its outlet was connected to a silica gel jar to remove moisture. Stopcocks, featuring a double oblique bore PTFE plug (2 mm), metrics ASAP 2020 V3.00H and smart instruments Co. Pvt. Ltd., SMART SORB 92/93, followed by closing the outlet.

Recovery of active sites in solid acid catalysts: The dye templated $AlSiO_4$ solid acid catalysts were used in the CO_2 decomposition reaction was collected and thoroughly calcinated at 450 ºC in a regeneration set-up.

RESULTS AND DISCUSSION

The produced non-porous solid acid catalysts were characterized using several analytical methods including FT-IR, TGA, DTG, DTA, TPD, BET and low angle XRD. SEM with EDX was used to investigate the surface morphology and chemical composition of catalysts.

Powder X-ray diffraction: The powder XRD technique was utilized to examine the crystallinity and mesosphere production. The formation of mesophase and crystallinity of the material is confirmed by XRD. Fig. 2 shows the intense peaks in the range of 2θ 0.5º to 2.5º. The planes are at 100, 110 and 200 with hexagonal symmetry [24-27]. The XRD patterns confirmed

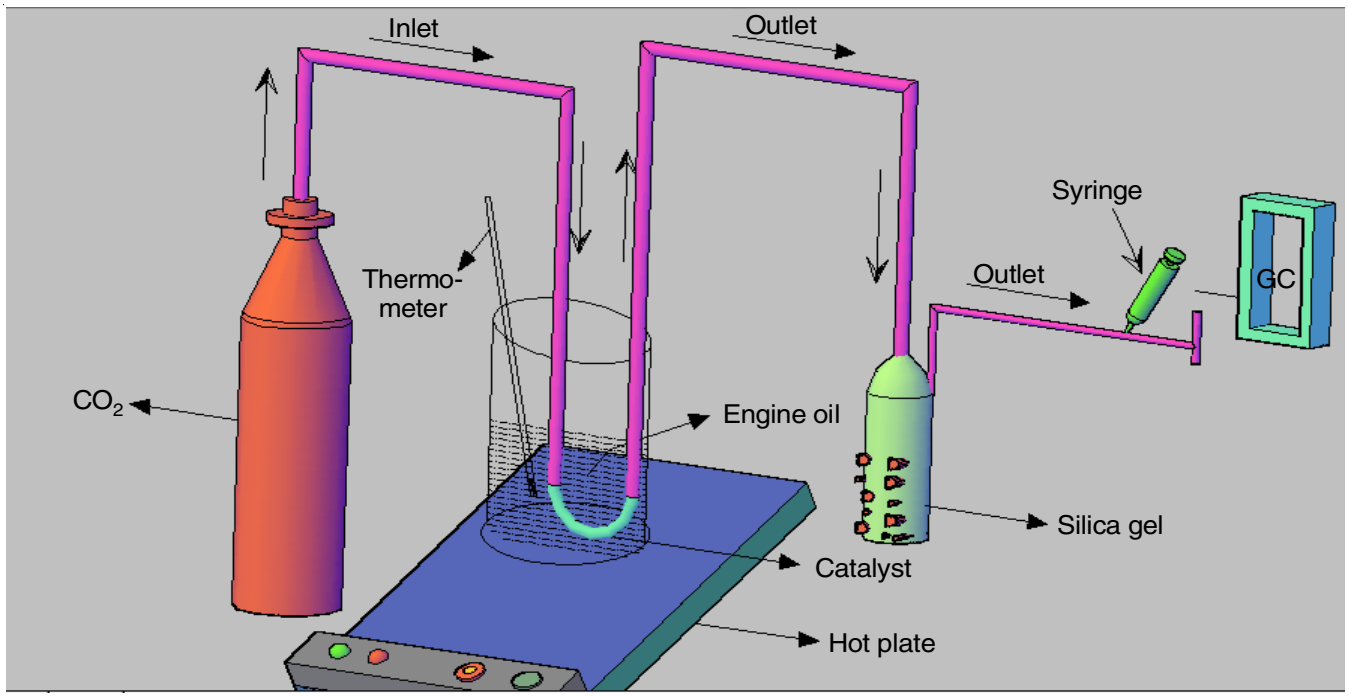

Fig. 1. U-type catalytic reactor

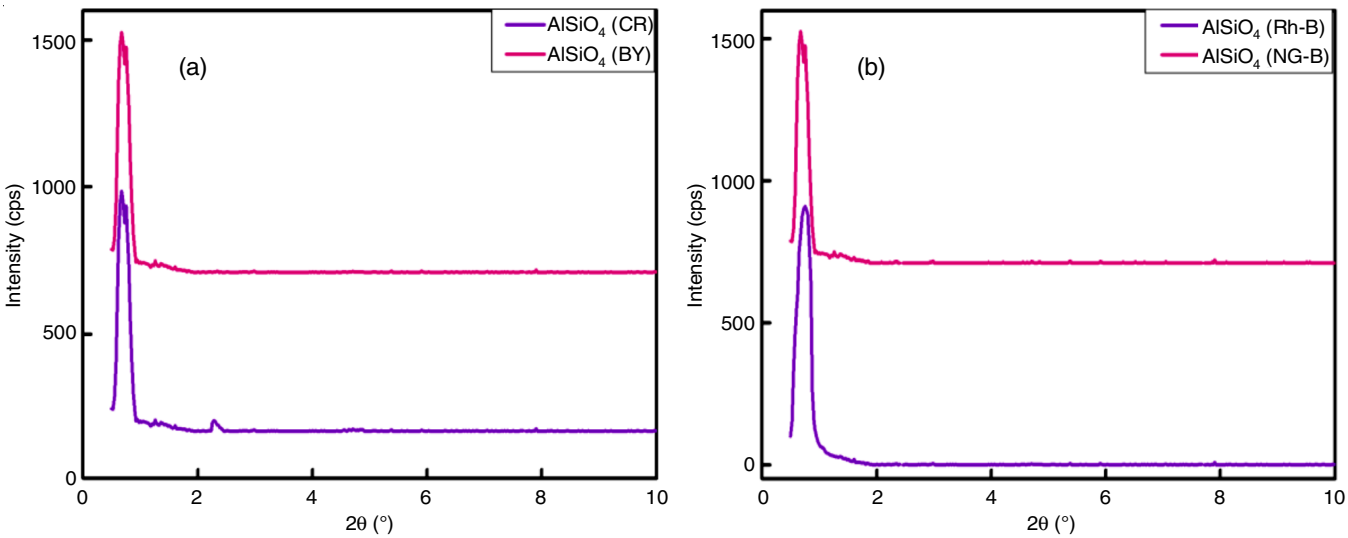

Fig. 2. Low angle XRD of $AlSiO_4$ ((a) cationic dye: Rh-B and nitroso dye: NG-B) and ((b) anionic dye: CR & BY)

that the prepared materials contain the highly ordered mesostructure with the templates [24-28].

FT-IR: FT-IR spectra of the as-synthesized and calcinated, anionic, nitroso and cationic dye templated aluminosilicate catalysts are shown in Fig. 3. In the as-synthesized materials, a strong band near 3500 cm^{-1} is due to the occurrence of water molecule (terminal –OH group), the bands of deformation, stretching and bending vibrations are observed in 1800-1200

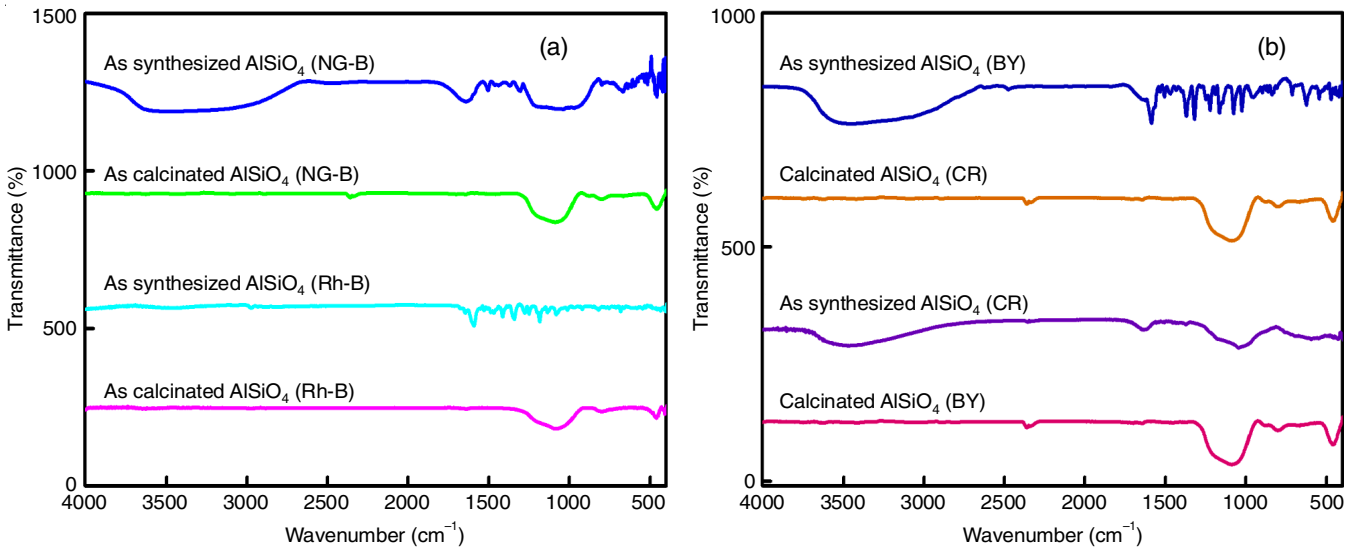

Fig. 3. FT-IR spectrum of as-synthesized & calcined $AlSiO_4$ with (a) cationic (Rh-B) & nitroso (NG-B) dye template and (b) anionic dye template

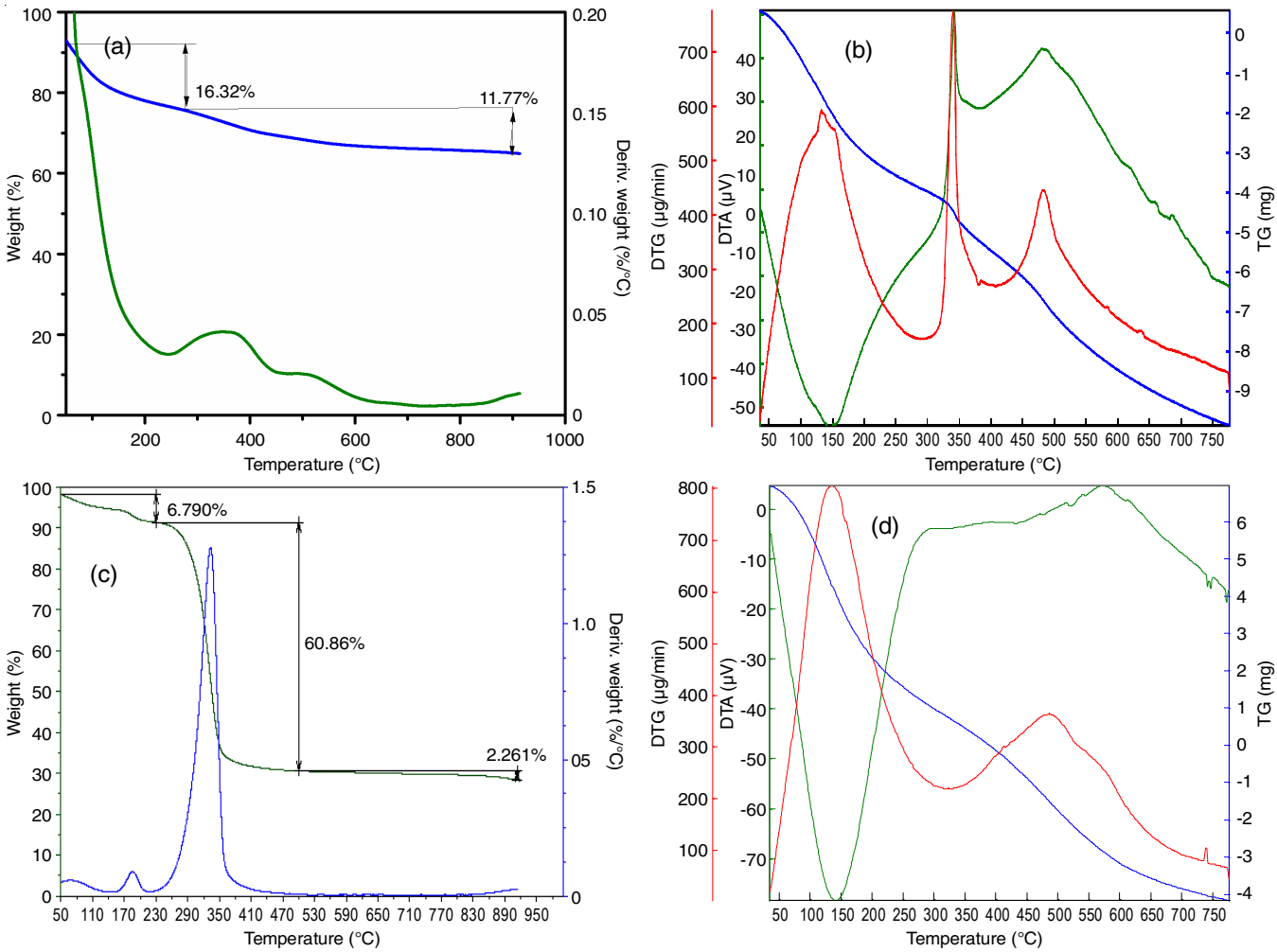

Fig. 4. TGA curve for as-synthesized $AlSiO_4$ (a) CR, (b) BY, (c) Rh-B and (d) NG-B

cm^{-1} range and due to its the existence of C-H, C-N, N-H, C-S bands. Due to the removal of templates from the material's pores and the absence of the peaks in the calcinated materials, these bands disappears after calcinations [24,29]. The asymmetric stretching and bending mode of the tetrahedral framework of $AlSiO_4$ is responsible for the strong symmetric bands around 1500 to 1100 cm^{-1} and the bending mode at 490 to 450 cm^{-1} [24,30-32]. Formation of the tetrahedral frameworks (Al-O-Si) is also confirmed by FT-IR spectrum. The tetrahedral framework maintains its strength and demonstrates stability even under high-temperature conditions.

Thermal studies: TGA is utilized to assess the thermal stability of the as-synthesized samples and Fig. 4 displays the thermograms of catalysts. Removal of water molecules and templates from the pores are monitored by TGA between the temperatures 50 to 950 ºC. TGA exhibits the first weight loss at 150 to 200 ºC with endothermic peaks due to the removal of physio-sorbed and chemi-sorbed water molecules from the surface of material [24,33,34]. The second weight (250-350 ºC) loss is caused by the decomposition of organic templates from the porous material and the peaks are exothermic in nature [24,35]. The final weight loss (above 500-800 ºC) is due to the elimination of adjacent –OH and silanol groups [36-38].

Temperature programmed desorption: Total acidity and active sites of the materials were analyzed by NH_3-TPD method and the TPD signals are shown in Fig. 5. The TPD was investigated in the temperature range of 100 to 800 ºC, from the TPD signal, $AlSiO_4$ (CR) has two active sites like Brønsted and Lewis [39,40], the material has the active sites at low temperature (250 ºC and 0.8037 mmol/g), so it can accelerate the reaction at low temperature itself. $AlSiO_4$ (BY) has 1.8111 mmol/g of acidity and it is active at 350 ºC, the broad peak indicated that it has strong, moderate and weak acid sites (200 to 780 ºC) [40]. The cationic and nitroso dye templated materials doesn't show any TPD signal, the signals are inverted. There are no active sites in $AlSiO_4$ (Rh-B and NG-B) and it has zero acidity [24]. In the cationic and nitroso dye templated materials, there is no possibility to create acidity it may be due to the reason of the positive charge of the dye molecules are balanced by negatively charged framework, as a result they have zero acidity and active sites (Table-2).

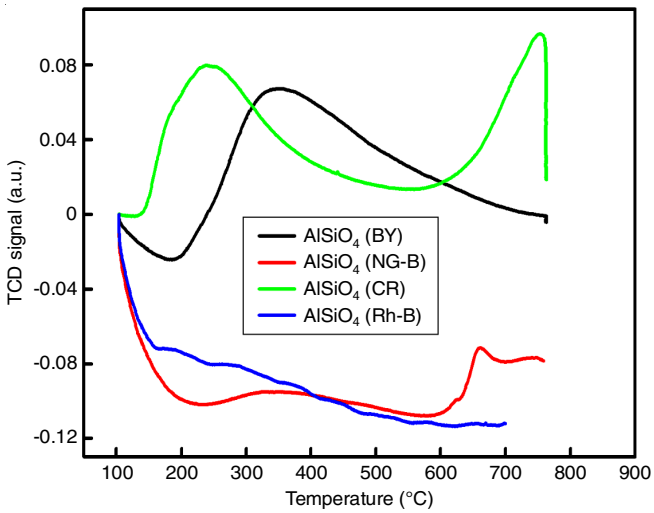

Fig. 5. NH_3 TPD for dye (CR, BY, NG-B and Rh-B) templated calcinated $AlSiO_4$

Adsorption isotherm: The N_2 adsorption-desorption isotherm was used to assess the porous character of the calcinated materials, as depicted in Fig. 6. In N_2 adsorption, the monolayer adsorption of nitrogen molecules on the mesoporous walls leads to the relative pressure $P/P_0 = 0.1$ to 0.9 and the capillary condensation of the material exhibits a type IV hysteresis loop [41,42]. Cationic and nitroso dyes templated $AlSiO_4$ material, can create same pore diameter, anionic dye molecules create different pore diameter. The textural parameters of the dye-templated materials were derived using the Brunauer-Emmett-Teller equations and are presented in Table-2.

Pore size, surface area and pore volume of $AlSiO_4$-13N and $AlSiO_4$-22 were analyzed by single point BET analyzer (SMART SORB 92/93) and it is shown in Fig. 7 and the results are given in Table-2. The following formula used to calculate pore size of the materials.

$$\text{Average pore diameter (Å)} = 40000 \times \frac{\text{Total pore volume (cc/g)}}{\text{Surface area (sq.m/g)}}$$

Nitroso and cationic dye templates are acting as a template but does not follow the micelle mechanism. These two templates follow different mechanism that may balance the negative charge of the framework by coordinating with aluminium sites. So these templates block the H^+ ions formation in the synthesis. Moreover, Congo red and brilliant yellow may follow the micelle mechanism. So, these two templates create acidity in the framework.

Morphological studies

SEM/EDX studies: The SEM analysis provides a detailed surface image of the calcinated minerals (Fig. 8). The porous characteristics, voids, particle clustering and the uneven textures of the materials are all clearly observable from this structural perspective [43,44]. The morphological changes may depend on the template micelle size. $AlSiO_4$-22 has needle shape particles and $AlSiO_4$-13N are spherical shape particles. In $AlSiO_4$-13R material, the pores are continuously connected with uniform spherical shape.

EDX analyzes the presence of components in the aluminosilicate framework. The presence of the distinctive signals of

TABLE-2
PHYSIOCHEMICAL CHARACTERISTICS OF DYE-TEMPLATED SOLID ACID CATALYSTS

Catalyst	Total acid (mmol/g)	S_{BET} (m^2/g)	W_{BJH}[a] (nm)	V_{meso} (cm^3/g)
$AlSiO_4$-15 (CR)	0.8037	43.9814	15.8	0.1849
$AlSiO_4$-22 (BY)	1.8111	7.6840	22.8	0.0438
$AlSiO_4$-13N (NG-B)	Nil	3.3790	13.3	0.0113
$AlSiO_4$-13R (Rh-B)	Nil	94.8800	13.1	0.3258

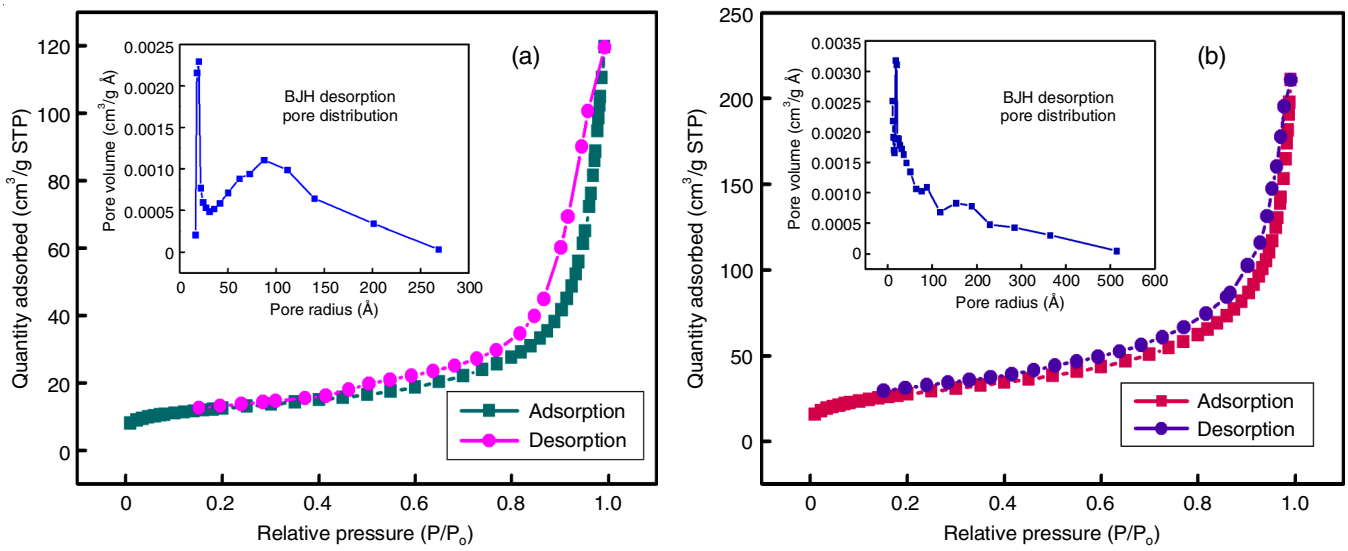

Fig. 6. N_2 sorption isotherm and pore size distribution of calcinated (a) $AlSiO_4$-13R and (b) $AlSiO_4$-15

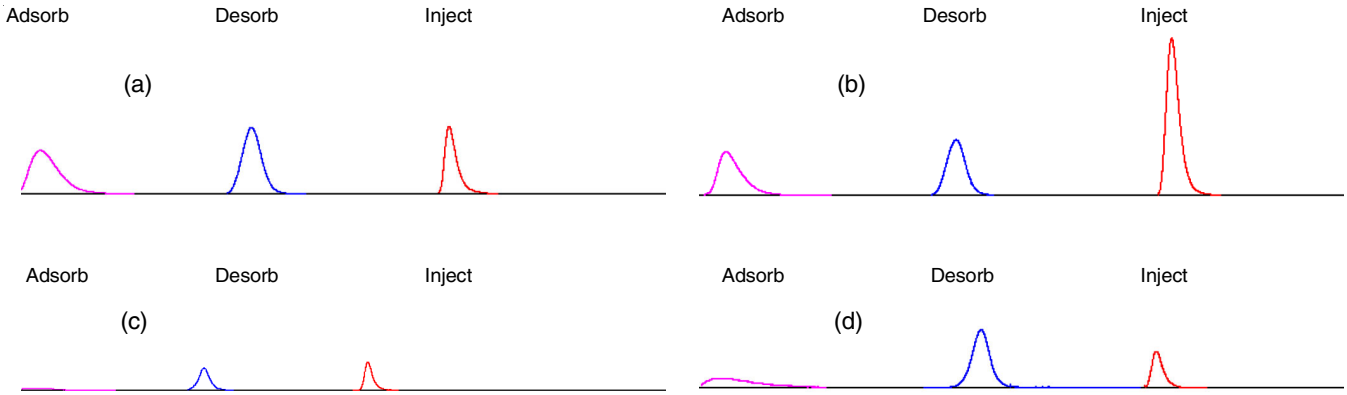

Fig. 7. Single point N_2 sorption isotherm of surface area of calcinated (a) $AlSiO_4$-22, (b) $AlSiO_4$-13N, pore volume of calcinated (c) $AlSiO_4$-22 and (d) $AlSiO_4$-13N

Al, O and Si in Fig. 9 was verified by EDX analysis. From EDX analysis, $AlSiO_4$-13R and $AlSiO_4$-13N has aluminum in the framework but in TPD it does not show any acid sites and the signals are inverted. This may be due to the template molecules coordinate with aluminium sites and prevent the H^+ ion formation and balancing of negative framework.

Decomposition of CO_2: An innovative catalytic reactor has been developed to breakdown CO_2. For the optimum conversion and selectivity, the maximal breakdown of CO_2 is adjusted by several parameters, including temperature, gas flow rate, catalyst dose and duration on stream.

Effect of temperature: Fig. 10 shows the temperature-dependent CO_2 decomposition process over $AlSiO_4$-13N, $AlSiO_4$-13R, $AlSiO_4$-15 and $AlSiO_4$-22 materials. Between 60 and 200 ºC, the temperature impact has been investigated. Table-3 provides a good representation of the CO_2 conversion % and its product selectivity as a function of temperature. The maximum conversion of carbon dioxide is found at 80 ºC for $AlSiO_4$-15 and $AlSiO_4$-22, further increase of temperature increases CO selectivity and decreases oxygen selectivity and partial decomposition.

$AlSiO_4$-13R exhibits activity at 60 ºC, but $AlSiO_4$-13N demonstrates activity at 80 ºC. Both catalysts exhibit maximum conversion at the optimized temperature; subsequent temperature increases result in a decline in both total and partial breakdown, as well as oxygen selectivity. The selectivity for carbon monoxide is increased.

Effect of flow rate: The materials are represented graphically in Fig. 11 and the impact of flow rate was investigated between 0.5 and 2.5 mL/min. All the materials exhibit high conversion at 0.5 mL/min; however, the prolonged residency of CO_2 molecules in the catalytic bed may be the cause of additional increases in flow rate, full and partial converion and oxygen selectivity (Table-4).

Effect of catalyst dosage: Fig. 12 illustrates the impact of catalyst loading on the decomposition of CO_2 in each of the four $AlSiO_4$ materials. Table-5 presents the findings of a study that examined the impact of catalyst loading between 0.5 and 2.5 g. With the exception of $AlSiO_4$-22, the maximum CO_2 conversion for $AlSiO_4$-15, $AlSiO_4$-13R and $AlSiO_4$-13N is observed at 0.5 g. The $AlSiO_4$-22 has large pore size, the conversion is very low. The catalytic dosage effect proved that the CO_2 decomposition slowly increased with increase of dosage.

Effect of time on stream: The catalyst's efficiency in breaking down carbon dioxide has been investigated over a period of one to 5 h. The effects of time on stream over dye

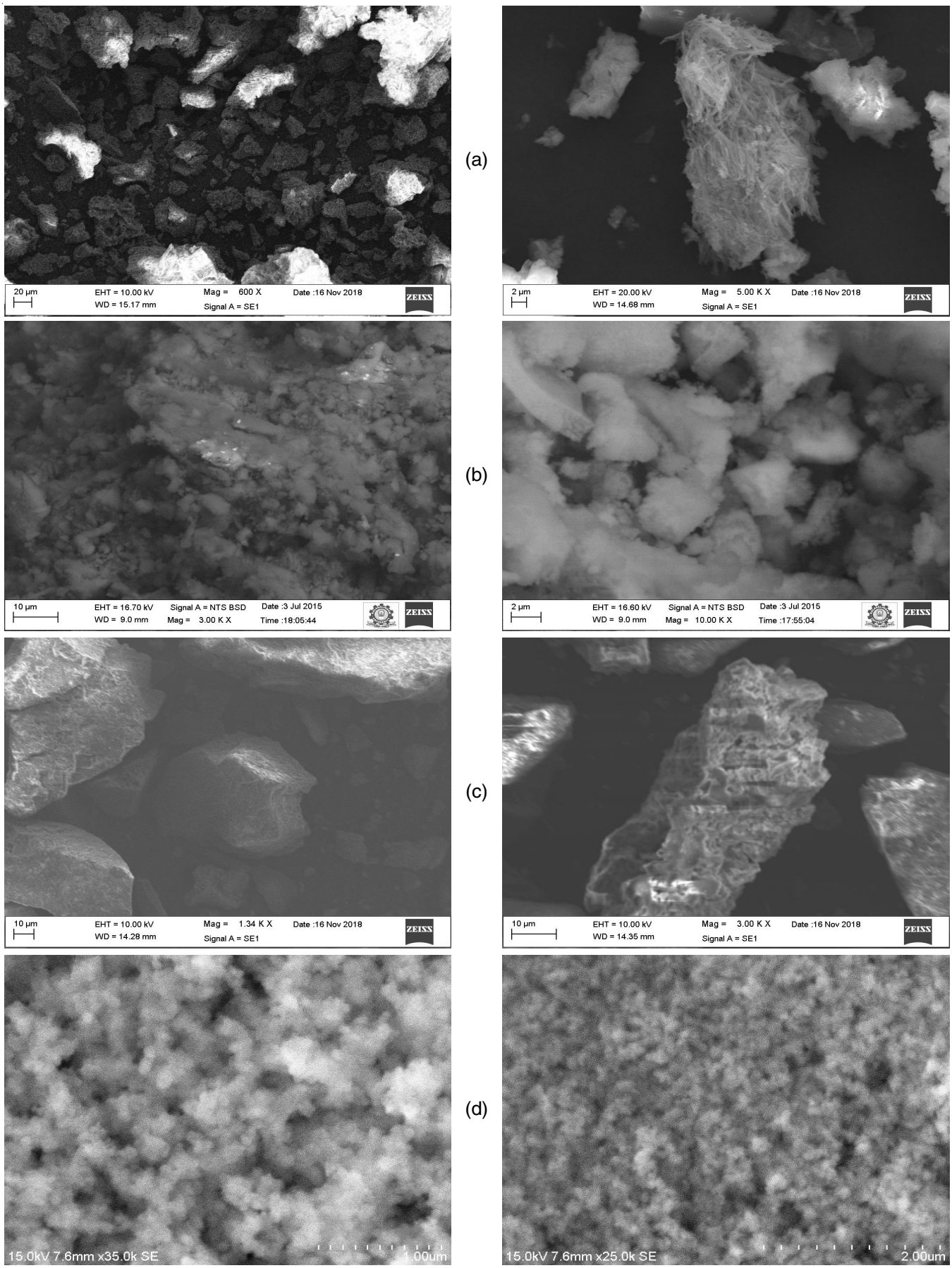

Fig. 8. SEM images of calcinated (a) $AlSiO_4$-22, (b) $AlSiO_4$-15, (c) $AlSiO_4$-13N and (d) $AlSiO_4$-13R

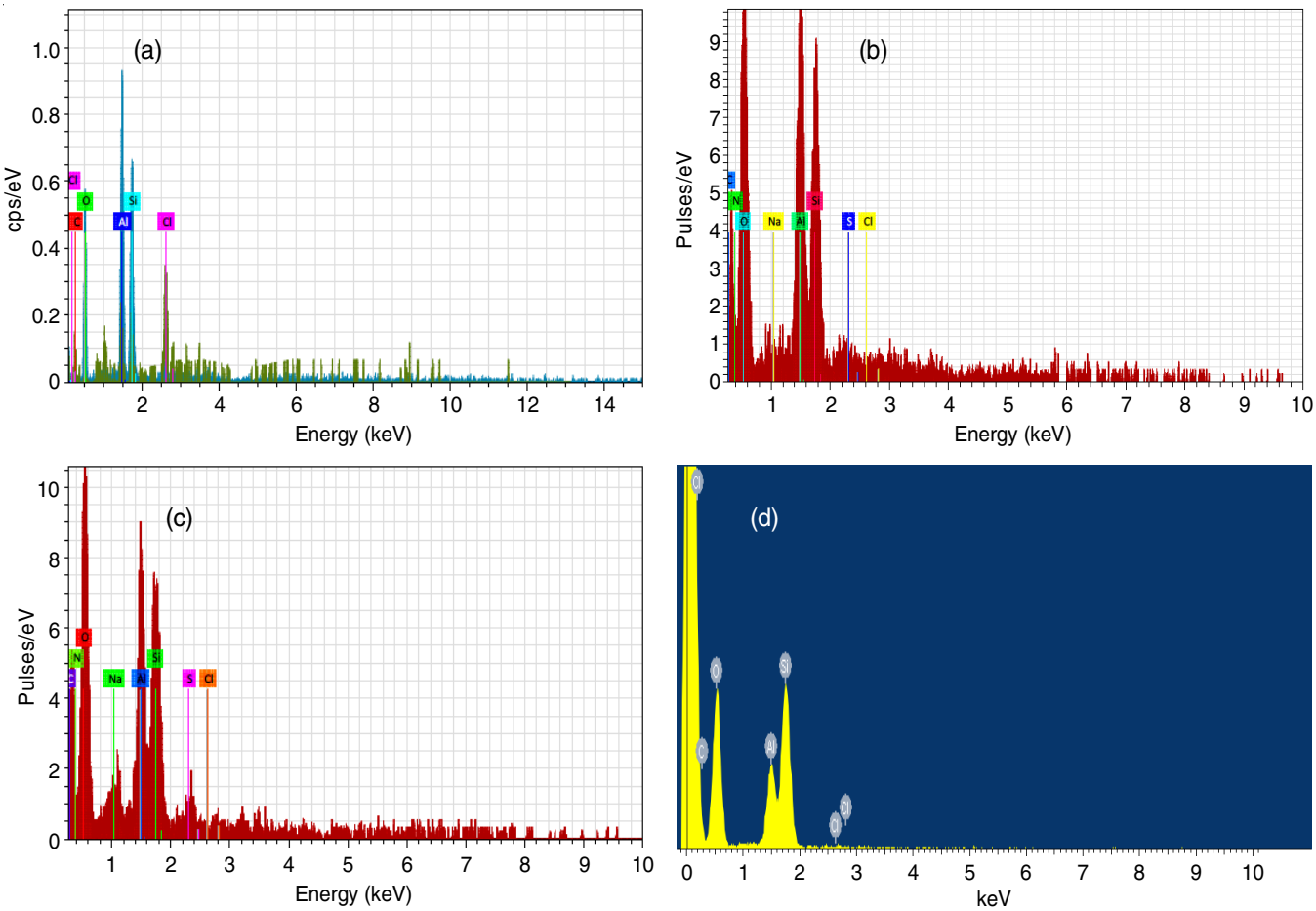

Fig. 9. EDX spectrum of calcinated (a) $AlSiO_4$-15, (b) $AlSiO_4$-22, (c) $AlSiO_4$-13N and (d) $AlSiO_4$-13R

TABLE-3
EFFECT OF TEMPERATURE ON CO_2 BREAKDOWN OVER $AlSiO_4$-15, $AlSiO_4$-22, $AlSiO_4$-13N AND $AlSiO_4$-13R

Catalyst	Temperature (ºC)	CO_2 conversion (%)			Product selectivity (%)	
		Complete decomposition	Partial decomposition	Total conversion	CO	O2
$AlSiO_4$-15	60	43	54	97	47	52
	70	44	54	98	47	52
	80	45	54	99	39	60
	100	60	13	73	47	52
	150	60	5	65	48	51
	200	56	4	60	60	39
$AlSiO_4$-22	60	1	8	9	29	70
	70	3	7	10	43	56
	80	11	8	19	42	57
	100	7	5	12	43	56
	150	1	5	6	50	49
	200	2	5	7	76	23
$AlSiO_4$-13R	60	62	30	92	46	53
	70	43	46	89	57	42
	80	7	60	67	56	43
	100	29	24	53	61	38
	150	25	23	48	69	29
	200	9	12	21	81	19
$AlSiO_4$-13N	60	22	3	25	88	11
	70	24	5	29	79	20
	80	35	4	39	88	11
	100	22	2	24	89	10
	150	18	2	20	94	5
	200	13	2	15	94	5

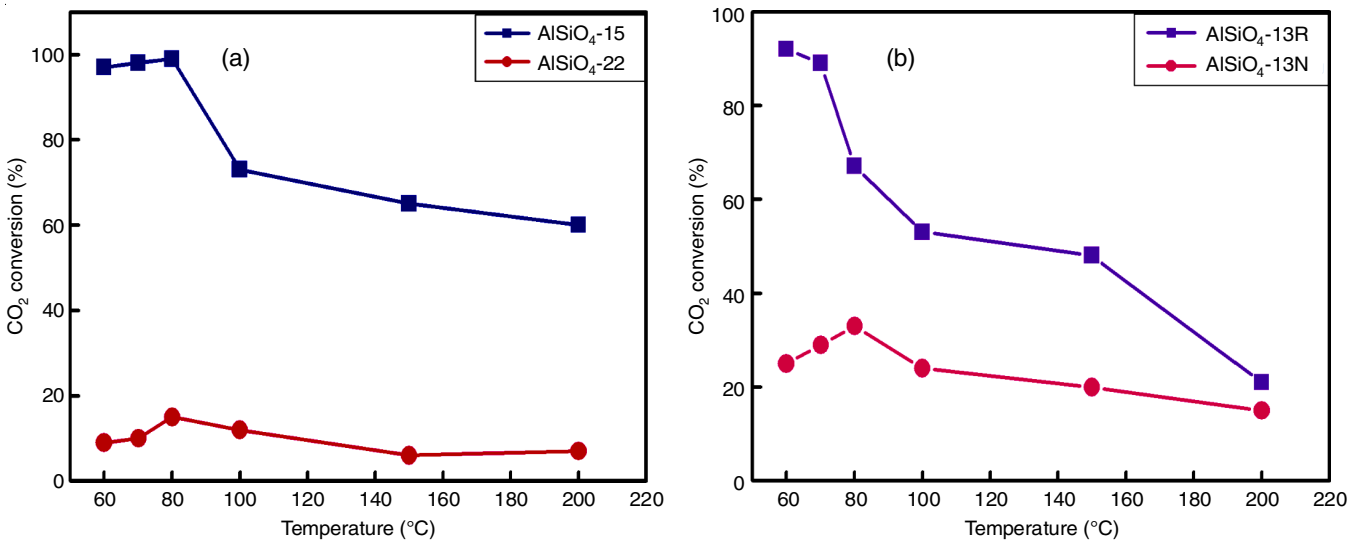

Fig. 10. Effect of temperature over (a) $AlSiO_4$-15 & $AlSiO_4$-22 and (b) $AlSiO_4$-13N & $AlSiO_4$-13R (dosage of catalyst: 0.5 g; flow rate: 0.5 mL/min; duration: 1 h)

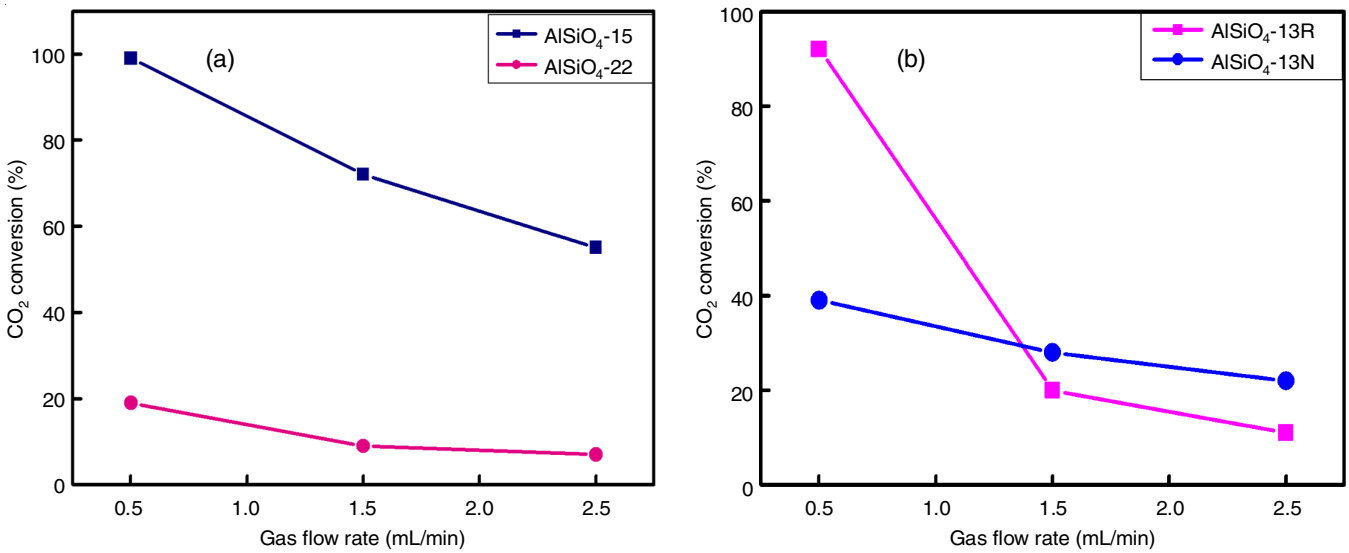

Fig. 11. Effect of gas flow rate over (a) $AlSiO_4$-15 & $AlSiO_4$-22 (duration: 1 h; temperature: $AlSiO_4$-15 & $AlSiO_4$-22 (80 ºC); catalyst dosage: 0.5 g) and (b) $AlSiO_4$-13R and $AlSiO_4$-13N's (dosage of catalyst: 0.5 g; temperatures of $AlSiO_4$-13R (60 ºC) and $AlSiO_4$-13N (80 ºC), duration: 1 h)

TABLE-4
FLOW RATE'S IMPACT ON CO_2 BREAKDOWN OVER $AlSiO_4$-15, $AlSiO_4$-22, $AlSiO_4$-13R AND $AlSiO_4$-13N

Catalyst	Flow rate (mL/min)	CO_2 conversion (%)			Product selectivity (%)	
		Complete decomposition	Partial decomposition	Total conversion	CO	O_2
$AlSiO_4$-15	0.5	45	54	99	39	60
	1.5	40	34	74	44	51
	2.5	35	23	58	45	54
$AlSiO_4$-22	0.5	11	8	19	8	91
	1.5	5	4	9	11	88
	2.5	3	4	7	29	70
$AlSiO_4$-13R	0.5	62	30	92	46	53
	1.5	9	11	20	82	17
	2.5	4	7	11	90	9
$AlSiO_4$-13N	0.5	35	4	39	79	20
	1.5	20	8	28	81	18
	2.5	19	3	22	89	6

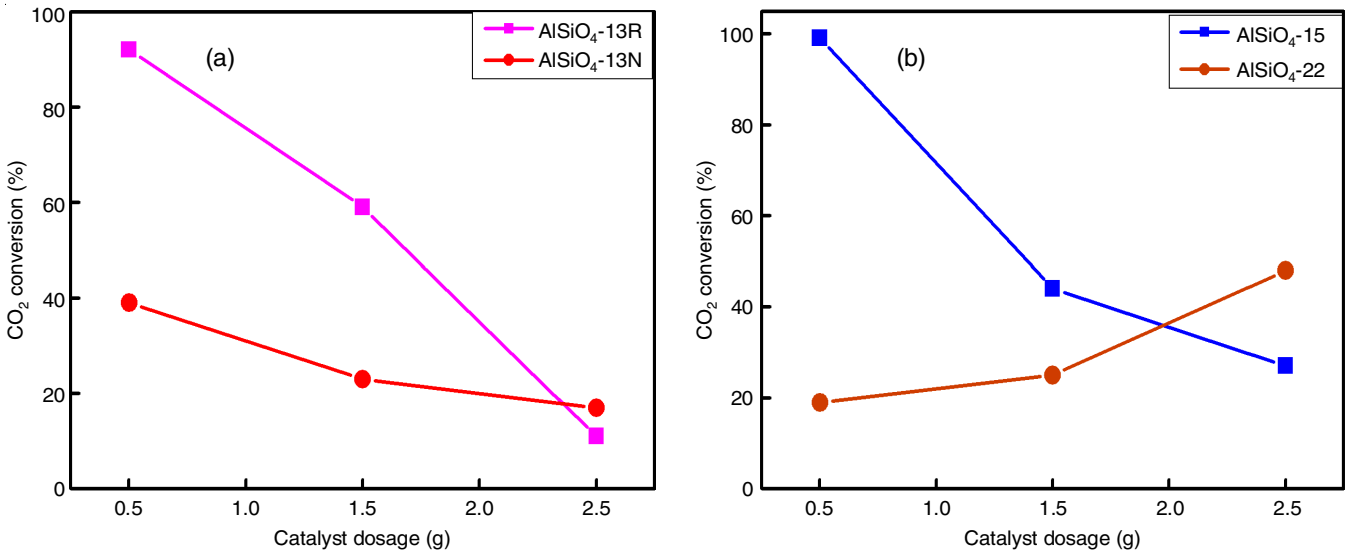

Fig. 12. Effect of catalyst dosage over (a) $AlSiO_4$-13R & $AlSiO_4$-13N (flow rate: 0.5 mL/min; temperature: 60 ºC for $AlSiO_4$-13R and 80 ºC for $AlSiO_4$-13N; duration: 1 h) and (b) $AlSiO_4$-15 and $AlSiO_4$-22 (flow rate: 0.5 mL/min; temperature: 75 ºC, duration: 1 h)

TABLE-5
CATALYST DOSAGE'S IMPACT ON CO_2 BREAKDOWN ACROSS $AlSiO_4$-15, $AlSiO_4$-22, $AlSiO_4$-13R AND $AlSiO_4$-13N

Catalyst	Catalyst dosage (g)	CO_2 conversion (%)			Product selectivity (%)	
		Complete decomposition	Partial decomposition	Total conversion	CO	O_2
$AlSiO_4$-15	0.5	45	54	99	39	60
	1.5	19	25	44	63	36
	2.5	18	9	27	84	15
$AlSiO_4$-22	0.5	11	8	19	29	70
	1.5	19	6	25	55	33
	2.5	21	27	48	27	72
$AlSiO_4$-13R	0.5	62	30	92	46	53
	1.5	35	24	59	70	29
	2.5	6	5	11	83	16
$AlSiO_4$-13N	0.5	35	4	39	79	20
	1.5	18	5	23	82	17
	2.5	16	1	17	84	15

templated $AlSiO_4$ materials are shown in Fig. 13. Percentage of conversion and product selectivity of the long time reaction is revealed in Table-6. As the amount of time on stream grew, carbon monoxide selectivity gradually rose and oxygen selectivity gradually fell. Partial and complete decomposition also decreased. The complete decomposition may result carbon and the carbon may deactivate the catalysts.

Complete decomposition of CO_2: $AlSiO_4$-15 and $AlSiO_4$-13R has shown the highest percentage of complete decomposition (Table-7). $AlSiO_4$-22 and $AlSiO_4$-13N has shown the lower percentage since the material has lower surface area. In these catalysts, surface area plays a major role for the maximum complete decomposition.

Carbon dioxide reaction mechanism: Carbon dioxide decomposes according to the method described below. CO_2 separates into CO and O in a gas phase reactor. The acidic site of the catalyst decomposes CO_2, yielding CO and O as by-products.

$$CO_2 \xrightarrow{\text{Catalytic cracking}} 2CO + O_2 \quad (1)$$

Carbon and oxygen are produced when CO is catalytically cracked.

$$2CO \longrightarrow 2C + O_2 \quad (2)$$

Two types of mechanisms are proposed and represented in **Schemes I** and **II**. $AlSiO_4$-13N and $AlSiO_4$-13R follows **Scheme-I** mechanism whereas the other two $AlSiO_4$ follows **Scheme-II** mechanism. **Scheme-II** oversees acidic-sited compounds, while **Scheme-I** describe the reaction pathways of non-acidic materials. The CO_2 molecule breaks down into the acidic materials to produce stable CO and O_2.

Conclusion

The mesoporous solid acid catalysts were synthesized by novel and inexpensive methods. First time waste dye effluents are used as a template for the synthesizing of nanoporous materials. The anionic dyes (Congo red and brilliant yellow), cationic dye (rhodamine-B) and nitroso dye (naphthol green-B) were used as a template. Several spectroscopic methods were used to characterize the produced nanoporous materials

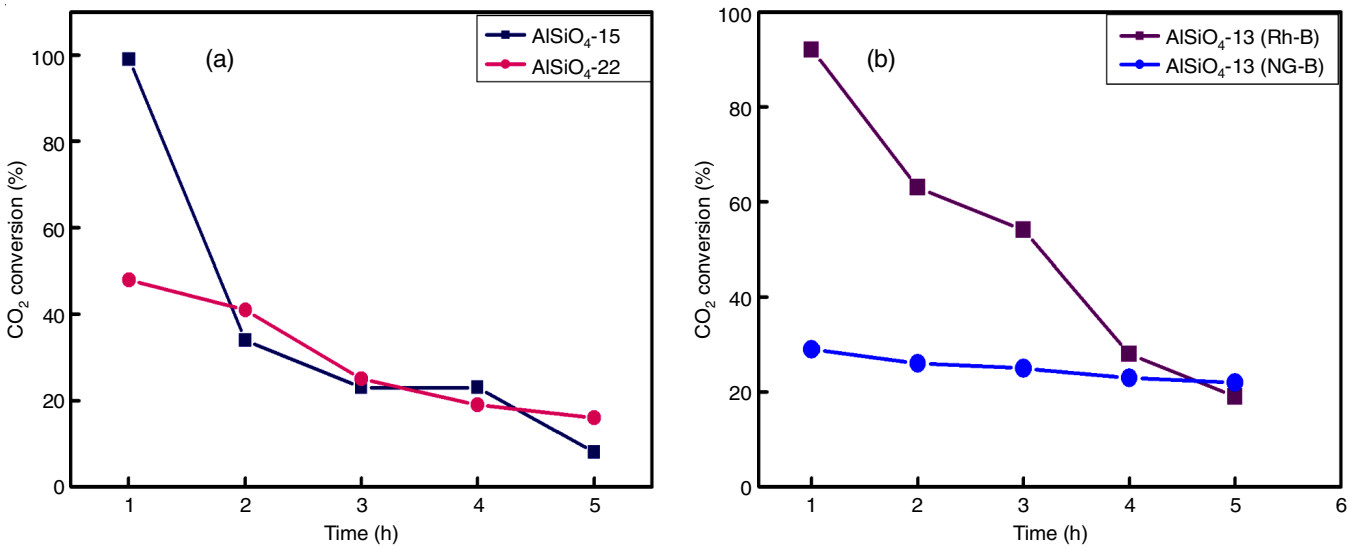

Fig. 13. The impact of time on the stream across (a) $AlSiO_4$-15 & $AlSiO_4$-22 [temperatures of $AlSiO_4$-15 and $AlSiO_4$-22 at 80 ºC); flow rate: 0.5 mL/min; dose of catalyst: $AlSiO_4$-22 (2.5 g), $AlSiO_4$-15 (0.5 g)] and (b) $AlSiO_4$-13R & $AlSiO_4$-13N [temperature: $AlSiO_4$-13R (60 ºC) & $AlSiO_4$-13N (80 ºC); flow rate: 0.5 mL/min; catalyst dosage: (0.5 g)]

TABLE-6
TIME'S IMPACT ON THE STREAM FOR CO_2 BREAKDOWN OVER $AlSiO_4$-15, $AlSiO_4$-22, $AlSiO_4$-13R AND $AlSiO_4$-13N

Catalyst	Contact time (h)	CO_2 conversion (%)			Product selectivity (%)	
		Complete decomposition	Partial decomposition	Total conversion	CO	O_2
$AlSiO_4$-15	1	45	54	99	39	60
	2	4	30	34	88	11
	3	1	22	23	93	6
	4	1	22	23	95	4
	5	2	6	8	72	27
$AlSiO_4$-22	1	21	27	48	27	72
	2	14	27	41	35	64
	3	15	10	25	38	61
	4	5	14	19	58	41
	5	7	9	16	74	25
$AlSiO_4$-13R	1	62	30	92	46	53
	2	39	24	63	20	79
	3	33	21	54	11	88
	4	15	13	28	9	90
	5	17	2	19	77	22
$AlSiO_4$-13N	1	35	4	39	79	20
	2	4	22	26	83	16
	3	3	22	25	88	11
	4	5	18	23	81	18
	5	2	20	22	89	10

TABLE-7
COMPLETE CARBON DIOXIDE BREAKDOWN ON $AlSiO_4$-15, $AlSiO_4$-22, $AlSiO_4$-13R AND $AlSiO_4$-13N

Catalyst	Optimized temperature (ºC)	Total acid (mmol/g)	S_{BET} (m^2/g) surface area	W_{BJH}[a] (nm) pore size	Complete CO_2 decomposition (%)
$AlSiO_4$-15	80	0.8037	43.9814	15.8	45
$AlSiO_4$-22	80	1.8111	7.6840	22.8	21
$AlSiO_4$-13N	80	Nil	3.3790	13.3	35
$AlSiO_4$-13R	60	Nil	94.8800	13.1	62

to verify their structural formation. The catalytic activity of the catalysts was investigated using the carbon dioxide breakdown method. In a catalytic reactor, temperature, flow rate, catalyst loading and time on stream were set to optimize CO_2 conversion during the catalytic reaction. In these catalysts, surface area plays a major role in the catalytic reaction. Compared with the conventional and reported methods the complete decomposition percentage of the material is high.

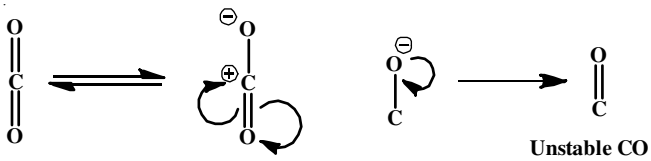

Scheme-I: Mechanism for non-acidic material

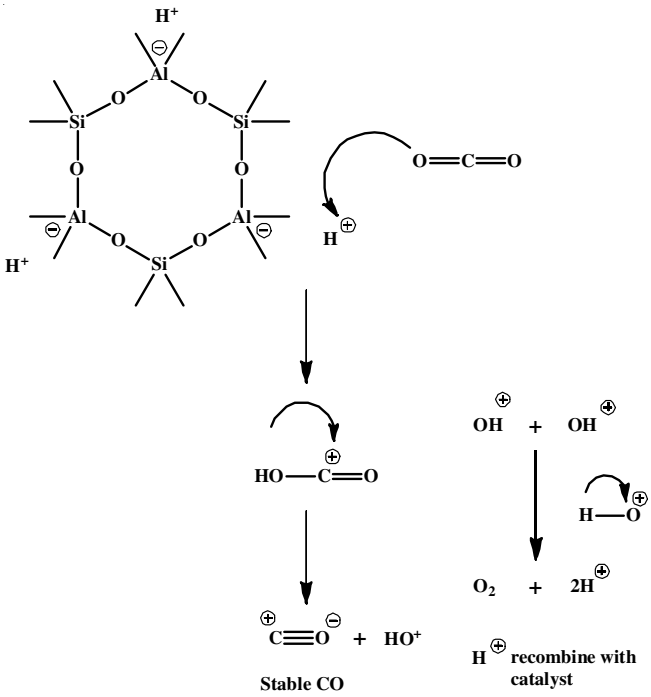

Scheme-II: Mechanism for acidic material

CONFLICT OF INTEREST

The authors declare that there is no conflict of interests regarding the publication of this article.

REFERENCES

1. K.-O. Kwak, S.-J. Jung, S.-Y. Chung, C.-M. Kang, Y. Huh and S.-O. Bae, *Biochem. Eng. J.*, **31**, 1 (2006); https://doi.org/10.1016/j.bej.2006.05.001
2. S.-Y. Chiu, C.-Y. Kao, C.-H. Chen, T.-C. Kuan, S.-C. Ong and C.-S. Lin, *Bioresour. Technol.*, **99**, 3389 (2008); https://doi.org/10.1016/j.biortech.2007.08.013
3. M.M. Maroto-Valer, Developments and Innovation in Carbon Dioxide (CO2) Capture and Storage Technology: Carbon Dioxide (CO2) Storage and Utilisation, Woodhead Publishing, edn. 1 (2010).
4. X. Xu, C. Song, J.M. Andresen, B.G. Miller and A.W. Scaroni, *Energy Fuels*, **16**, 1463 (2002); https://doi.org/10.1021/ef020058u
5. C. Nordhei, K. Mathisen, I. Bezverkhyy and D. Nicholson, *J. Phys. Chem. C*, **112**, 6531 (2008); https://doi.org/10.1021/jp7112158
6. R.D. Richardson, E.J. Holland and B.K. Carpenter, *Nat. Chem.*, **3**, 301 (2011); https://doi.org/10.1038/nchem.1000
7. T. Nunnally, K. Gutsol, A. Rabinovich, A. Fridman, A. Gutsol and A. Kemoun, *J. Phys. D Appl. Phys.*, **44**, 274009 (2011); https://doi.org/10.1088/0022-3727/44/27/274009
8. D. Ray and C. Subrahmanyam, *RSC Adv.*, **6**, 39492 (2016); https://doi.org/10.1039/C5RA27085E
9. D. Mei, X. Zhu, Y.-L. He, J.D. Yan and X. Tu, *Plasma Sources Sci. Technol.*, **24**, 15011 (2014); https://doi.org/10.1088/0963-0252/24/1/015011
10. J. Wang, L. Huang, R. Yang, Z. Zhang, J. Wu, Y. Gao, Q. Wang, D. O'Hare and Z. Zhong, *Energy Environ. Sci.*, **7**, 3478 (2014); https://doi.org/10.1039/C4EE01647E
11. M. Ding, R.W. Flaig, H.-L. Jiang and O.M. Yaghi, *Chem. Soc. Rev.*, **48**, 2783 (2019); https://doi.org/10.1039/C8CS00829A
12. R. Ben-Mansour, M.A. Habib, O.E. Bamidele, M. Basha, N.A.A. Qasem, A. Peedikakkal, T. Laoui and M. Ali, *Appl. Energy*, **161**, 225 (2016); https://doi.org/10.1016/j.apenergy.2015.10.011
13. C. Jia, K. Dastafkan, W. Ren, W. Yang and C. Zhao, *Sustain. Energy Fuels*, **3**, 2890 (2019); https://doi.org/10.1039/C9SE00527G
14. V. Jiménez, A. Ramírez-Lucas, J. Antonio-Díaz, P. Sánchez and A. Romero, *Environ. Sci. Technol.*, **46**, 7407 (2012); https://doi.org/10.1021/es2046553
15. C. Kannan, K. Sivakami and J.I. Jeyamalar, *Mater. Lett.*, **113**, 93 (2013); https://doi.org/10.1016/j.matlet.2013.08.129
16. S.M. Solberg, D. Kumar and C.C. Landry, *J. Phys. Chem. B*, **109**, 24331 (2005); https://doi.org/10.1021/jp054187y
17. Y. Liu and T.J. Pinnavaia, *J. Am. Chem. Soc.*, **125**, 2376 (2003); https://doi.org/10.1021/ja029336u
18. C. Kannan, K. Muthuraja and M.R. Devi, *J. Hazard. Mater.*, **244-245**, 10 (2013); https://doi.org/10.1016/j.jhazmat.2012.11.016
19. K.J. Edler, P.A. Reynolds, J.W. White and D. Cookson, *J. Chem. Soc., Faraday Trans.*, **93**, 199 (1997); https://doi.org/10.1039/a605676h
20. D. Fan, P. Tian, S. Xu, Q. Xia, X. Su, L. Zhang, Y. Zhang, Y. He and Z. Liu, *J. Mater. Chem.*, **22**, 6568 (2012); https://doi.org/10.1039/c2jm15281a
21. C. Yu, H. Chu, Y. Wan and D. Zhao, *J. Mater. Chem.*, **20**, 4705 (2010); https://doi.org/10.1039/b925864g
22. Y. Wan, Y. Shi and D. Zhao, *Chem. Commun.*, 897 (2007); https://doi.org/10.1039/B610570J
23. E. Masika and R. Mokaya, *Chem. Mater.*, **23**, 2491 (2011); https://doi.org/10.1021/cm200706n
24. M.A.M. Thangam, J.I. Jeyamalar and C. Kannan, *J. Chem. Pharm. Sci.*, **9**, 2460 (2016).
25. C.-Y. Chen, H.-X. Li and M.E. Davis, *Micropor. Mater.*, **2**, 17 (1993); https://doi.org/10.1016/0927-6513(93)80058-3
26. P. Yang, D. Zhao, D.I. Margolese, B.F. Chmelka and G.D. Stucky, *Chem. Mater.*, **11**, 2813 (1999); https://doi.org/10.1021/cm990185c
27. M. Selvaraj, P.K. Sinha, K. Lee, I. Ahn, A. Pandurangan and T.G. Lee, *Micropor. Mesopor. Mater.*, **78**, 139 (2005); https://doi.org/10.1016/j.micromeso.2004.10.004
28. R. Srinivasan, R.A. Keogh and B.H. Davis, *Appl. Catal. A Gen.*, **130**, 135 (1995); https://doi.org/10.1016/0926-860X(95)00127-1
29. A. Galarneau, D. Desplantier-Giscard, F. Di Renzo and F. Fajula, *Catal. Today*, **68**, 191 (2001); https://doi.org/10.1016/S0920-5861(01)00300-5
30. K. Góra-Marek and J. Datka, *Appl. Catal. A Gen.*, **302**, 104 (2006); https://doi.org/10.1016/j.apcata.2005.12.027
31. S.N.A. Shafie, W.X. Liew, M. Nordin, N.A. Hadi, M.R. Bilad, N. Sazali, Z.A. Putra and M.D.H. Wirzal, *Adv. Polym. Technol.*, **2019**, 2924961 (2019); https://doi.org/10.1155/2019/2924961
32. A. Vinu, T. Krithiga, V. Murugesan and M. Hartmann, *Adv. Mater.*, **16**, 1817 (2004); https://doi.org/10.1002/adma.200400229
33. D.P. Serrano, J.M. Escola and P. Pizarro, *Chem. Soc. Rev.*, **42**, 4004 (2013); https://doi.org/10.1039/C2CS35330J
34. A. Vinu, D.P. Sawant, K. Ariga, K.Z. Hossain, S.B. Halligudi, M. Hartmann and M. Nomura, *Chem. Mater.*, **17**, 5339 (2005); https://doi.org/10.1021/cm050883z

35. N.I. Taib, S. Endud and M.N. Katun, *Int. J. Chem.*, **3**, 2 (2011); https://doi.org/10.5539/ijc.v3n3p2
36. M. Hino and K. Arata, *Catal. Lett.*, **30**, 25 (1995); https://doi.org/10.1007/BF00813669
37. A. Corma and V. Fornes, *Stud. Surf. Sci. Catal*., **135**, 73 (2001); https://doi.org/10.1016/S0167-2991(01)81187-3
38. P.Y. Chen, S.J. Chu, N.S. Chang, T.K. Chuang and L.Y. Chen, *Stud. Surf. Sci. Catal*., 46m 231 (1989); https://doi.org/10.1016/S0167-2991(08)60980-5
39. D.O. de Zárate, F. Bouyer, H. Zschiedrich, P.J. Kooyman, P. Trens, J. Iapichella, R. Durand, C. Guillem and E. Prouzet, *Chem. Mater.*, **20**, 1410 (2008); https://doi.org/10.1021/cm7024558
40. A. Belhakem and A. Bengueddach, *Bull. Chem. Soc. Ethiop.*, **20**, 99 (2006).
41. B. Zhang, X. Li, Q. Wu, C. Zhang, Y. Yu, M. Lan, X. Wei, Z. Ying, T. Liu, G. Liang and F. Zhao, *Green Chem.*, **18**, 3315 (2016); https://doi.org/10.1039/C5GC03077C
42. A.V. Vijayasankar, N. Mahadevaiah, Y.S. Bhat and N. Nagaraju, *J. Porous Mater.*, **18**, 369 (2011); https://doi.org/10.1007/s10934-010-9387-z
43. D. Tian, W. Yan, X. Cao, J. Yu and R. Xu, *Chem. Mater.*, **20**, 2160 (2008); https://doi.org/10.1021/cm703317c
44. C.-X. Gui, Q.-Q. Wang, S.-M. Hao, J. Qu, P.-P. Huang, C.-Y. Cao, W.-G. Song and Z.-Z. Yu, *ACS Appl. Mater. Interfaces*, **6**, 14653 (2014); https://doi.org/10.1021/am503997e